Supporting Information

Influence of Phosphate Species on Peroxymonosulfate Activation by Copper-Cobalt Dual-Atom Biochar for Sulfamethoxazole Degradation

Chuanbin Wang[a,1], Yang Hu[a,1], Ning Li[b], Hailin Tian[a], Xiaoyu Wu[c], Jingnan Tian[b], Tianyuan Zhang[a], Yixi Xie[a], Daying Chen[b], Changchun Xin[b], Yanpeng Cai[a], Xiaoqiang Cui[b], Guanyi Chen[b,d], Qian Tan[a*]

[a] Guangdong Basic Research Center of Excellence for Ecological Security and Green Development, Guangdong Provincial Key Laboratory of Water Quality Improvement and Ecological Restoration for Watersheds, School of Ecology, Environment and Resources, Guangdong University of Technology, Guangzhou, 510006, China.

[b] School of Environmental Science and Engineering, Tianjin University, Tianjin 300072, PR China

[c] School of Chemistry and Chemical Engineering, Yangzhou University, Yangzhou 225002, P. R. China

[d] School of Mechanical Engineering, Tianjin University of Commerce, Tianjin 300134, P. R. China

[*] Corresponding Author:

qian_tan@gdut.edu.cn (Qian Tan)

Text S1

Chemicals: SMX and PMS were obtained from Shanghai Nine-Ding Chemistry Co., Ltd. Orthoboric acid (H_3BO_3), sodium tetraborate decahydrate ($Na_2B_4O_7 \cdot 10H_2O$), acetic acid ($C_2H_4O_2$), sodium thiosulfate pentahydrate ($Na_2S_2O_3 \cdot 5H_2O$) were purchased from Shanghai Aladdin Biochemical Technology Co., Ltd. Tert-butylalcohol (TBA), methanol (MeOH), L-histidine (L-his), trichloromethane ($CHCl_3$), copper nitrate hydrate ($Cu(NO_3)_2 \cdot 3H_2O$), cobaltous nitrate hexahydrate ($Co(NO_3)_2 \cdot 6H_2O$), zinc sulfate hydrate ($H_{12}N_2O_{12}Zn$), dicyandiamide ($C_2H_4N_4$), sulfuric acid (H_2SO_4) were provided by Tianjin Heowns Biochemical Technology Co., Ltd. All chemicals used are analytically pure.

Text S2

Synthesis methods of copper-cobalt dual-atom decorated biochar: Firstly, the distilled water (500 mL) was placed in a beaker, and then added zinc sulfate hydrate (20 mM) and copper nitrate hydrate/cobaltous nitrate hexahydrate (12.5 mM). After fully dissolved, 4 g dried cow manure was added and stirred, and the precursor was obtained after drying. Then, the precursor and dicyandiamide were put in a mortar and thoroughly ground in a 1:10 mass ratio. The catalyst preparation process was set at 550°C for 1 h, then increased to 950°C at a rate of 10 °C/min and held for 1 h. Sulfuric acid was applied to remove excess metal ions in the biochar. In NBC-Cu-Co, the mass ratio of Cu supported precursor to Co supported precursor was 1:1.

Text S3

Characterization methods: X-ray photoelectron spectroscopy (XPS, ESCALAB 250Xi+K-alpha, USA) was used to detect the relative elements. The SMX concentration was detected by a high-performance liquid chromatography (HPLC, Agress 1100) with a 254 nm UV detector and a C18 column (4.6 mm × 150 mm × 5 μm). The gradient elution was conducted at a flow rate of 1.0 $mL \cdot min^{-1}$ with methanol as the A mobile phase and phosphoric acid (0.1 wt%) as the B mobile phase. The mobile phase adopted a linear program from 90% B to 90% B in 0–3 min, 90% B to 40% B in 3–5 min, 40% B in 5–10 min, 40% B to 90% B in 10–15 min, 90% B in 15–18 min. Quencher concentrations were as follows: tert-butanol at 200 times the PMS concentration, methanol at 200 times the PMS concentration, chloroform at 30 times the PMS concentration, and L-histidine at 20 times the PMS concentration."

Text S4

DFT calculation method： The density functional theory (DFT) calculations were carried out with the VASP code (Kresse and Furthmüller, 1996). The Perdew–Burke–Ernzerhof (PBE) functional within generalized gradient approximation (GGA)(Perdew et al., 1996) was used to process the exchange–correlation, while the projectoraugmented-wave pseudopotential (PAW)(Blochl, 1994) was applied with a kinetic energy cut-off of 500 eV, which was utilized to describe the expansion of the electronic eigenfunctions. The vacuum thickness was set to be 25 Å to minimize interlayer interactions. The Brillouin-zone integration was sampled by a Γ-centered 5 ×

5 × 1 Monkhorst–Pack k-point. All atomic positions were fully relaxed until energy and force reached a tolerance of 1×10^{-5} eV and 0.03 eV/Å, respectively. The dispersion corrected DFT-D method was employed to consider the long-range interactions(Grimme, 2006). Employing the climbing image nudged elastic band method (CI-NEB), we computed the minimum energy pathway of the cyclization reaction along with its corresponding activation barrier.

The adsorption energy (E_{ads}) of a complex formed between two molecules, A and B, can be calculated using the following equation:

$$E_{ads} = E_{complex} - (E_A + E_B) \quad (S1)$$

Where:

$E_{complex}$ is the total energy of the molecular complex of A and B.

E_A and E_B are the total energies of isolated molecules A and B, respectively.

The Gibbs free energy change (ΔG) was calculated by computational hydrogen electrode (CHE) model as follows:

$$\Delta G = \Delta E + \Delta ZPE - T\Delta S \quad (S2)$$

here ΔE is the reaction energy obtained by the total energy difference between the reactant and product molecules absorbed on the catalyst surface and ΔS is the change in entropy for each reaction, ΔZPE is the zero-point energy correction to the Gibbs free energy. T represents room temperature (298.15 K).

Text S5

The basis for calculating the contribution of reactive species: “The second-order

rate constants of quenching ·OH, $SO_4^{\cdot-}$, and $^1O_2$ by L-His are 5.0×10^9, 2.5×10^9, and 3.2-5.0×10^7 $M^{-1}s^{-1}$, respectively (Ren et al., 2021). Contributions of ·OH (λ(·OH)) and $SO_4^{\cdot-}$ (λ($SO_4^{\cdot-}$)) species to SMX degradation were calculated by **Eqs. (S3, S4)**. Obviously, L-His could quench ·OH, $SO_4^{\cdot-}$, and $^1O_2$. Hence, the $^1O_2$ contribution (λ($^1O_2$)) can be calculated by **Eq. S5.** In addition, the $O_2^{\bullet-}$ contribution was obtained by **Eq. S6.** Besides, the rate constant for a unit mass of metal is calculated as the rate constant for the total free radicals divided by the metal content of the biochar.

$$\lambda(\cdot OH) = (k_0-k_1)/k_0\times100\% \quad (S3)$$

$$\lambda(SO_4^{\cdot-}) = (k_1-k_2)/k_0\times100\% \quad (S4)$$

$$\lambda(^1O_2) = (k_2-k_3)/k_0\times100\% \quad (S5)$$

$$\lambda(O_2^{\bullet-}) = (k_0-k_4)/k_0\times100\% \quad (S6)$$

Where k_0, k_1, k_2, k_3, k_4 present the pseudo-first-order rate constants of biochar/PMS, biochar/PMS/TBA, biochar/PMS/MeOH, biochar/PMS/L-his and biochar/PMS/$ClCH_3$ systems."

Text S6

Under acidic conditions, the chemical efficiency was less than 1, indicating that a portion of PMS was consumed unproductively (e.g., via side reactions or water oxidation). In contrast, the chemical efficiency was mostly greater than 1 under neutral and alkaline conditions, suggesting the presence of chain-propagating radical amplification effects.

Text S7

XPS analysis: The C 1s spectrum could be separated into four components: C-OH, C-C/C=C, COOH and C=O at ~285.4 eV, ~284.6 eV, ~288.7 eV and ~286.3 eV (Wang et al., 2023a). The O 1s peak was divided into C=O, C-O and O-C=O groups at ~531.0 eV, ~531.6 eV and ~532.6 eV, respectively (Wang et al., 2019). For the N 1s peak, three characteristic peaks at ~398.6 eV, ~399.8 eV, and ~400.8 eV were identified as pyridinic N, pyrrolic N and graphitic N in biochars (Wang et al., 2023b). Three valence states of Cu species were determined: Cu^0 (951.6 eV), Cu^+ (934.7 eV and 953.5 eV) and Cu^{2+} (932.5 eV and 952.8 eV) (Sun et al., 2023; Wang et al., 2024). In addition, the high-resolution Co 2p spectrum was divided into five peaks. The peak at 779.0 eV were indexed to Co^0 (Zhu et al., 2022), two peaks at 781.2 eV and 796.7 eV were identified as Co^{2+}, and the peaks at 794.9 eV and 779.7 eV were attributed to Co^{3+} (Cai et al., 2022).

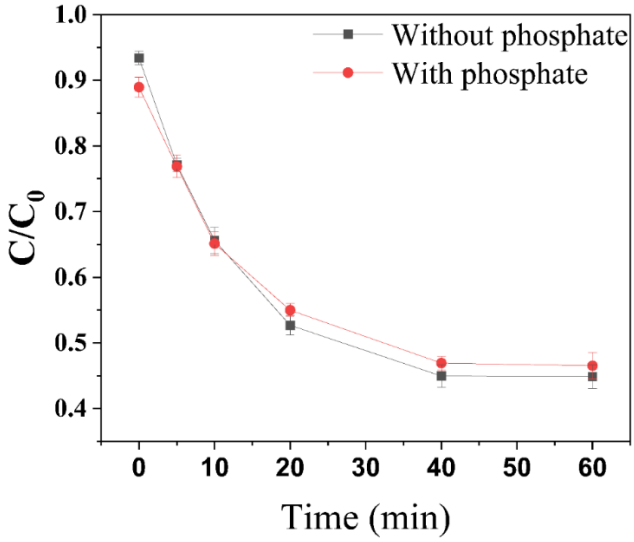

Fig. S1 Furfuryl alcohol degradation efficiency in the presence of biochar without phosphate and with phosphate. (C(Biochar) = 0.02 g/L; [PMS] = 1.2 mM; C(Furfuryl alcohol) = 10 μM; Stable pH= 4; T=25 ℃, C (phosphate) = 5 mM).

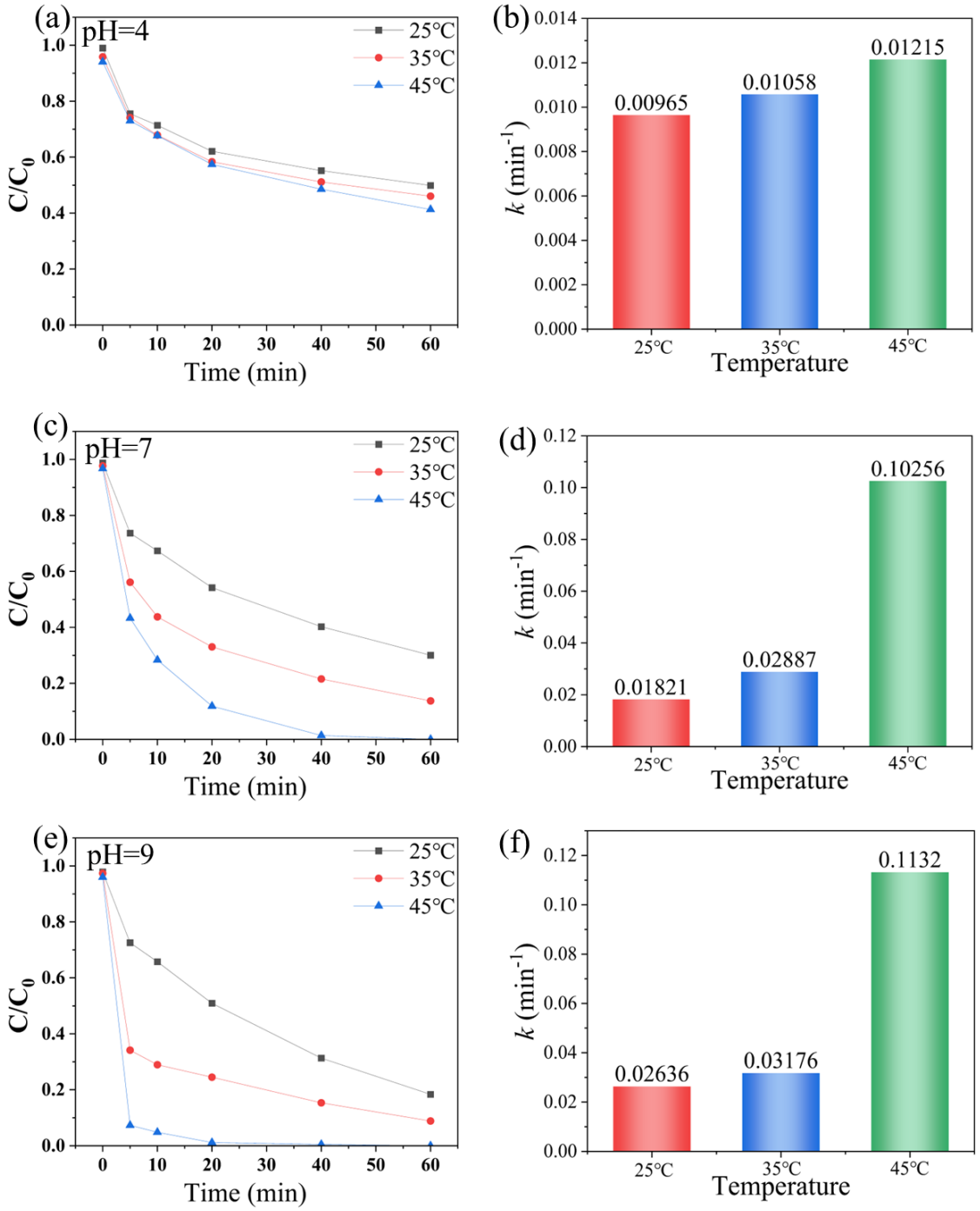

Fig. S2 SMX degradation efficiency in the presence of phosphate under different pH (pH =4(a-b), pH=7(c-d), pH=9(e-f). Conditions: C(NBC-Cu-Co) = 0.02 g/L, [PMS] = 1.2 mM, $[SMX]_0$ =15 mg/L, $[Phosphate]_0$ = 5 mM.

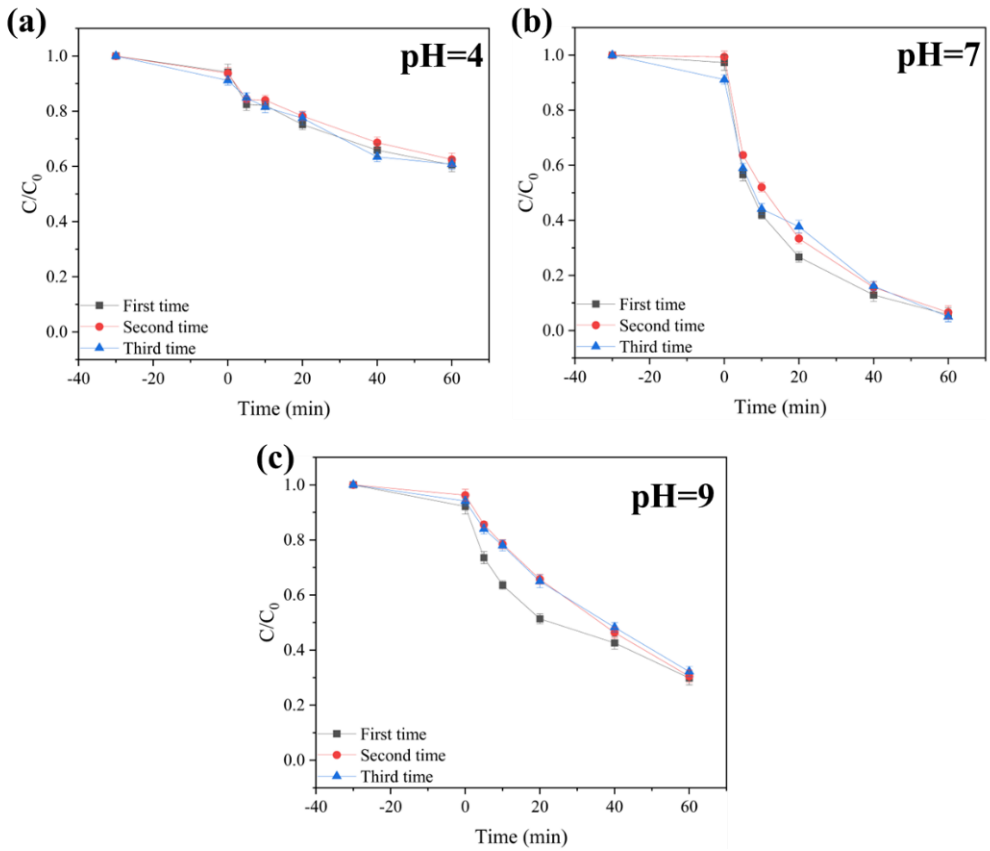

Fig. S3 SMX degradation efficiency in the presence of phosphate under different pH (pH =4(a), pH =7(b), pH =9(c). Conditions: C(NBC-Cu-Co) = 0.02 g/L, [PMS] = 1.2 mM, $[SMX]_0$ =15 mg/L.

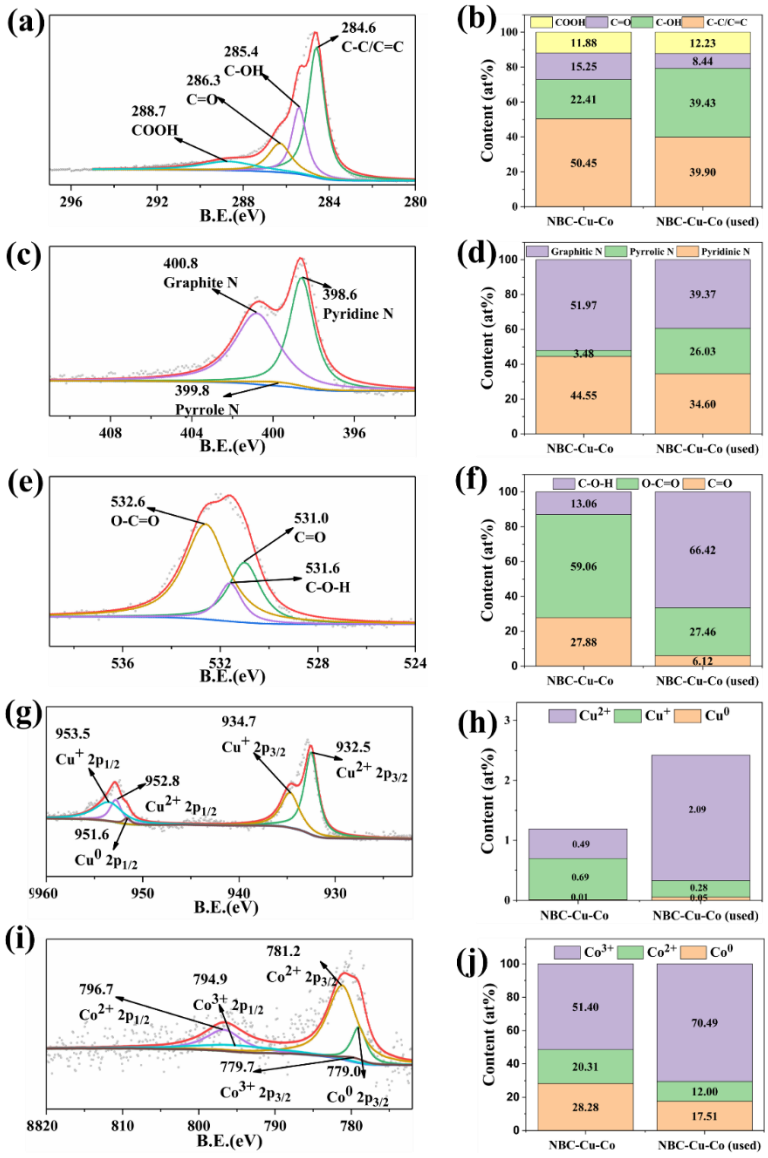

Fig. S4 High resolution XPS spectra of different elements: (a) C, (c) N, (e) O, (g) Cu and (i) Co. The contents of different related active sites of (b) C element, (d) N element, (f) O element, (h) Cu element, and (j) Co element;

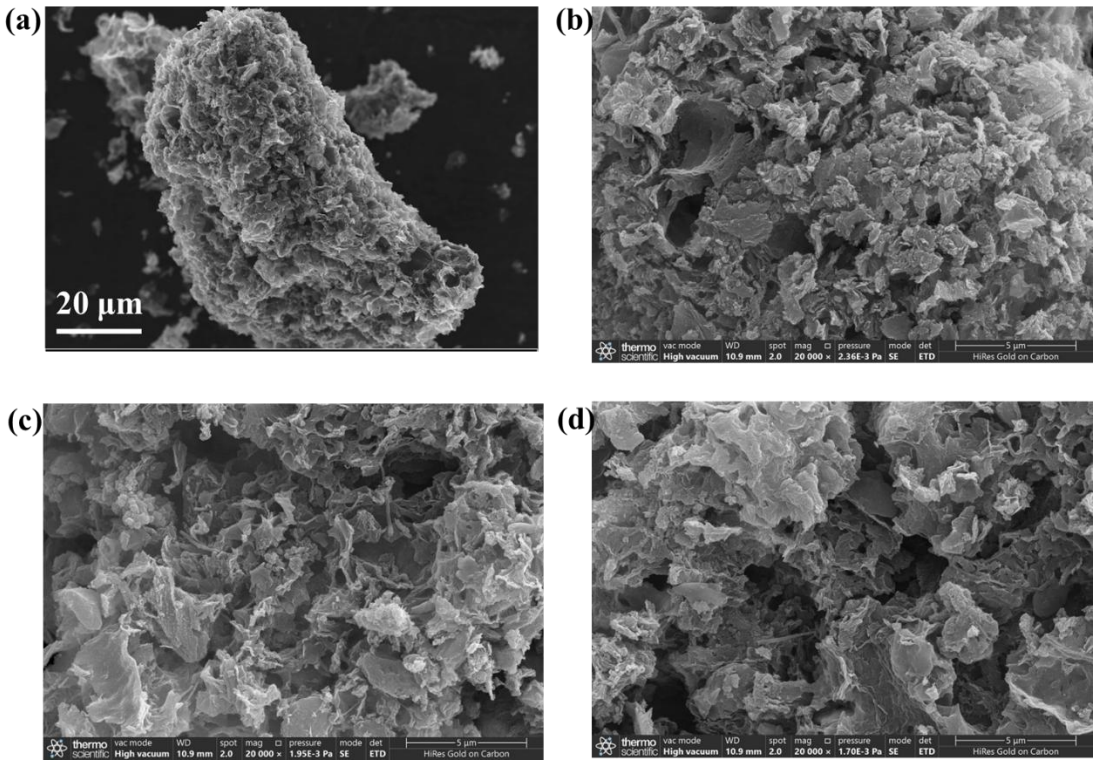

Fig. S5. Scanning electron microscope (SEM) of (a) NBC-Cu-Co and after reaction under the condition of pH=4(b), pH=7(c), pH=9(d).

Table S1 The observed rate constant (k_{obs}), along with its error bars and goodness-of-fit under acidic conditions in the presence of $H_2PO_4^-$.

	K_{obs} (without biochar)	Error bars	R-square	K_{obs} (with biochar)	Error bars	R-square
0 mM	0.0026	8.2E-5	0.90935	0.0083	8.2E-5	0.88556
5 mM	0.0027	8.9E-5	0.95011	0.0082	9.1E-5	0.96402
10 mM	0.0024	9.4E-5	0.92759	0.0085	9.5E-5	0.8565
15 mM	0.0023	8.8E-5	0.91153	0.0085	8.9E-5	0.87912
20 mM	0.0026	7.8E-5	0.94802	0.0084	7.9E-5	0.94383

Table S2 The observed rate constant (k_{obs}), along with its error bars and goodness-of-fit under alkaline conditions in the presence of HPO_4^{2-}.

	K_{obs} (without biochar)	Error bars	R-square	K_{obs} (with biochar)	Error bars	R-square
0 mM	0.0062	8.1E-5	0.99067	0.0129	2.2E-4	0.98976
5 mM	0.0073	9.2E-5	0.99908	0.0161	2.3E-4	0.9948
10 mM	0.0088	9.5E-5	0.99728	0.0282	1.8E-4	0.99761
15 mM	0.0093	8.9E-5	0.99962	0.0341	3.1E-4	0.99651
20 mM	0.0105	7.7E-5	0.99851	0.0364	3.2E-4	0.99208

Table S3 The observed rate constant (k_{obs}), along with its error bars and goodness-of-fit under neutral conditions in the presence of HPO_4^{2-} and $H_2PO_4^-$.

	K_{obs} (without biochar)	Error bars	R-square	K_{obs} (with biochar)	Error bars	R-square
0 mM	0.0065	8.2E-5	0.92557	0.0397	8.1E-5	0.99834
5 mM	0.0072	9.3E-5	0.92544	0.0445	9.1E-5	0.99258
10 mM	0.0066	9.4E-5	0.95674	0.0421	9.6E-5	0.99074
15 mM	0.0066	8.8E-5	0.96049	0.0348	8.9E-5	0.99597
20 mM	0.0066	7.8E-5	0.95869	0.0268	7.9E-5	0.99784

Table S4 The observed rate constant (k_{obs}) and its normalized value under acidic conditions in the presence of $H_2PO_4^-$.

	K_{obs} (without biochar) [min^{-1}]	K_{norm} [$min^{-1} \cdot m^{-2}$]	K_{obs} (with biochar) [min^{-1}]	K_{norm} (with) [$min^{-1} \cdot m^{-2}$]
0 mM	0.0026	0.01256	0.0083	0.04010
5 mM	0.0027	0.01304	0.0082	0.03961
10 mM	0.0024	0.01159	0.0085	0.04106
15 mM	0.0023	0.01111	0.0085	0.04106
20 mM	0.0026	0.01256	0.0084	0.04058

Table S5 The observed rate constant (k_{obs}) and its normalized value under alkaline conditions in the presence of HPO_4^{2-}.

	K_{obs} (without biochar) [min^{-1}]	K_{norm} [$min^{-1} \cdot m^{-2}$]	K_{obs} (with biochar) [min^{-1}]	K_{norm} (with) [$min^{-1} \cdot m^{-2}$]
0 mM	0.0062	0.02995	0.0129	0.06232
5 mM	0.0073	0.03527	0.0161	0.07778
10 mM	0.0088	0.04251	0.0282	0.13623
15 mM	0.0093	0.04493	0.0341	0.16473
20 mM	0.0105	0.05072	0.0364	0.17585

Table S6 The observed rate constant (k_{obs}) and its normalized value under neutral conditions in the presence of HPO_4^{2-} and $H_2PO_4^-$.

	K_{obs} (without biochar) [min^{-1}]	K_{norm} [$min^{-1}\cdot m^{-2}$]	K_{obs} (with biochar) [min^{-1}]	K_{norm} (with) [$min^{-1}\cdot m^{-2}$]
0 mM	0.0065	0.03140	0.0397	0.19179
5 mM	0.0072	0.03478	0.0445	0.21498
10 mM	0.0066	0.03188	0.0421	0.20338
15 mM	0.0066	0.03188	0.0348	0.16812
20 mM	0.0066	0.03188	0.0268	0.12947

Table S7 The chemical efficiency under neutral conditions (ΔSMX/ΔPMS)

	ΔSMX	ΔPMS	ΔSMX/ΔPMS
25℃	0.037705	0.0403	0.93560356
35℃	0.046092	0.0074	6.22860637
45℃	0.053095	0.0133	3.99213999

Table S8 The chemical efficiency under acidic conditions (ΔSMX/ΔPMS)

	SMX	PMS	ΔSMX/ΔPMS
25℃	0.026469	0.1018	0.260013
35℃	0.026839	0.0922	0.291094
45℃	0.028439	0.0871	0.326514

Table S9 The chemical efficiency under alkaline conditions (ΔSMX/ΔPMS)

	SMX	PMS	ΔSMX/ΔPMS
25℃	0.046791	0.0149	3.140345
35℃	0.052092	0.0196	2.657746
45℃	0.056499	0.0113	4.999937

Table S10 The turnover frequency (TOF) per metal site under different conditions.

	TOF_Cu –$H_2PO_4^-$	TOF_Cu – HPO_4^{2-}	TOF_Cu – HPO_4^{2-}+ $H_2PO_4^-$	TOF_Co – TOF_Co –$H_2PO_4^-$	TOF_Co – HPO_4^{2-}	TOF_Co – HPO_4^{2-}+ $H_2PO_4^-$
0 mM	0.0913	0.1420	0.4369	0.3082	0.4790	1.4741
5 mM	0.0902	0.1772	0.4897	0.3045	0.5978	1.6523
10 mM	0.0935	0.3103	0.4633	0.3156	1.0471	1.5632
15 mM	0.0935	0.3752	0.3829	0.3156	1.2661	1.2921
20 mM	0.0925	0.4005	0.2949	0.3119	1.3515	0.9951

Table S11 Metal leaching concentration in cyclic experiments under acidic conditions

pH=4	Co (μg/L)	Cu (μg/L)
First cycle	12.22	22.68
Second cycle	5.93	21.07
Third cycle	4.40	15.68

Table S12 Metal leaching concentration in cyclic experiments under neutral conditions

pH=7	Co (μg/L)	Cu (μg/L)
First cycle	8.47	28.39
Second cycle	7.54	36.17
Third cycle	8.95	28.35

Table S13 Metal leaching concentration in cyclic experiments under alkaline conditions

pH=9	Co (μg/L)	Cu (μg/L)
First cycle	17.52	13.28
Second cycle	6.00	10.28
Third cycle	6.46	16.08

References:

Blochl, P.E., (1994). Projector augmented-wave method. Phys Rev B Condens Matter 50(24), 17953-17979.

Cai, P., Zhao, J., Zhang, X., Zhang, T., Yin, G., Chen, S., Dong, C.-L., Huang, Y.-C., Sun, Y., Yang, D., Xing, B., (2022). Synergy between cobalt and nickel on NiCo2O4 nanosheets promotes peroxymonosulfate activation for efficient norfloxacin degradation. Applied Catalysis B: Environmental 306, 121091.

Grimme, S., (2006). Semiempirical GGA-type density functional constructed with a long-range dispersion correction. J Comput Chem 27(15), 1787-1799.

Kresse, G., Furthmüller, J., (1996). Efficiency of ab-initio total energy calculations for

metals and semiconductors using a plane-wave basis set. Computational Materials Science 6(1), 15-50.

Perdew, J.P., Burke, K., Ernzerhof, M., (1996). Generalized Gradient Approximation Made Simple. Phys. Rev. Lett. 77(18), 3865-3868.

Ren, W., Cheng, C., Shao, P., Luo, X., Zhang, H., Wang, S., Duan, X., (2021). Origins of Electron-Transfer Regime in Persulfate-Based Nonradical Oxidation Processes.

Sun, J., Zhang, D., Xia, D., Li, Q., (2023). Orange peels biochar doping with Fe-Cu bimetal for PMS activation on the degradation of bisphenol A: A synergy of SO4−, OH, 1O2 and electron transfer. Chemical Engineering Journal 471, 144832.

Wang, C., Dai, H., Liang, L., Li, N., Cui, X., Yan, B., Chen, G., (2023a). Enhanced mechanism of copper doping in magnetic biochar for peroxymonosulfate activation and sulfamethoxazole degradation. Journal of Hazardous Materials 458, 132002.

Wang, C., Liang, L., Cui, Y., Cui, X., Li, N., Cheng, Z., Yan, B., Chen, G., (2023b). The influence of monohydrogen and dihydrogen phosphates on peroxymonosulfate activation by Enteromorpha magnetic biochar for sulfamethoxazole degradation. Separation and Purification Technology 324, 124586.

Wang, S., Xu, L., Wang, J., (2019). Nitrogen-doped graphene as peroxymonosulfate activator and electron transfer mediator for the enhanced degradation of sulfamethoxazole. Chemical Engineering Journal 375, 122041.

Wang, Y., Qiao, L., Zhang, X., Liu, Z., Li, T., Wang, H., (2024). Green synthesis of FeCu@biochar nanocomposites through a mechanochemical method for enhanced

tetracycline degradation via peroxymonosulfate activation. Separation and Purification Technology 328, 125077.

Zhu, H., Guo, A., Wang, S., Long, Y., Fan, G., Yu, X., (2022). Efficient tetracycline degradation via peroxymonosulfate activation by magnetic Co/N co-doped biochar: Emphasizing the important role of biochar graphitization. Chemical Engineering Journal 450, 138428.